

From reaction kinetics to dementia: a simple dimer model of Alzheimer's disease etiology

Michael R. Lindstrom^{a,1}, Manuel B. Chavez^a, Elijah A. Gross-Sable^a, Eric Y. Hayden^{b,c}, and David B. Teplow^{b,c}

^aDepartment of Mathematics, University of California, Los Angeles, 520 Portola Plaza, Math Science Building, Room 6363, Los Angeles, CA 90095, United States;

^bDepartment of Neurology, David Geffen School of Medicine at UCLA, 635 Charles E. Young Drive South, Room 445, Los Angeles, CA 90095, United States; ^cMolecular Biology Institute and Brain Research Institute, University of California, Los Angeles, CA 90095

This manuscript was compiled on November 1, 2019

Oligomers of the amyloid β -protein ($A\beta$) have been implicated in the pathogenesis of Alzheimer's disease (AD) through their toxic action on neurons. Understanding the process of oligomerization may contribute to the development of therapeutic agents, but this has been difficult due to the complexity of oligomerization and the metastability of the oligomers thus formed. One means to overcome these difficulties is to develop models of the oligomerization process. Here, we use experimental data from cell viability assays and proxies for rate constants involved in monomer-dimer-trimer kinetics to develop a simple mathematical model linking $A\beta$ assembly to oligomer-induced neuronal degeneration. This model recapitulates the rapid growth of disease incidence with age. It does so through incorporation of age-dependent changes in rates of $A\beta$ monomer production and elimination. The model also describes clinical progression in genetic forms of AD (e.g., Down's syndrome), changes in hippocampal volume, AD risk after traumatic brain injury, and spatial spreading of the disease due to foci in which $A\beta$ production is elevated. Continued incorporation of clinical and basic science data into the current model will make it an increasingly relevant model system for doing experiments that are not feasible in biological systems. In addition, terms in the model that have particularly large effects are likely to be especially useful therapeutic targets.

amyloid β -protein | Alzheimer's disease | oligomers | mathematical modeling | etiology

Alzheimer's disease (AD) currently is the 6th leading cause of death in the U.S. and its prevalence continues increasing rapidly (1). Thus there is a critical need for the development of effective preventive, ameliorative, or curative therapeutics. Unfortunately, none exist (2). A reason why is the multifactorial nature of AD, which makes contemporaneous study of the entire system infeasible and requires researchers to focus on smaller system elements. One such element is amyloid plaque formation. Plaques in the brains of those with AD are extracellular deposits of long protein fibrils formed by the amyloid β -protein ($A\beta$) and one of the pathognomonic features of AD. This inspired the hypothesis that fibril formation is the seminal pathologic event in AD, an event that leads to neuronal injury, death, and clinical signs (memory loss) (3). However, this "amyloid cascade hypothesis," has largely been supplanted by the "oligomer cascade hypothesis," which suggests that pre-fibrillar structures, oligomers, are the most important toxic agents (4). Like AD itself, the process by which monomeric $A\beta$ forms fibrils is complicated and involves a multitude of small, oligomeric assemblies, as well as large, pre-fibrillar precursor structures (5). It has been suggested that oligomers as small as dimers may be the most important

of these assemblies (6).

$A\beta$ oligomerization and its effect on neurons in vitro and in vivo are being studied intensively (for recent reviews, see (7, 8)). Studies in our group (9) and others (10–12) have focused on the structural biology and kinetics of oligomerization and fibril formation. These studies have sought to relate these biophysical aspects of $A\beta$ assembly to disease occurrence, pathology, and progression. The results have provided insight into the conformational features important for $A\beta$ assembly and toxicity and how these features control assembly kinetics. Much less is known about the relationship of particular oligomer states to the clinical development of disease. It is clear that the constitutive level of $A\beta$ production correlates directly with time of onset and severity of disease. This is particularly apparent in people with Down's syndrome, who possess three copies of the amyloid precursor protein gene that encodes $A\beta$. Simple gene dosage extrapolation suggests that $A\beta$ should be produced at 150% the level found in normal individuals. However, studies by Cheon *et al.* (13) have shown that immunoreactive APP species are expressed in Down's syndrome brains at levels up to 3-fold higher. Higher $A\beta$ expression also is observed in rare familial forms of AD that are characterized by mutations in APP or the enzymes responsible for its production (14). These mutations result in increased concentrations of $A\beta$ or an increase in the relative

Significance Statement

Oligomeric assemblies of $A\beta$ are hypothesized to be seminal pathologic agents in Alzheimer's disease (AD). Mechanistic studies of oligomerization and neurotoxicity in humans are currently impossible, yet such studies promise to advance efforts toward target identification and drug development. To overcome this hurdle, we developed a simple, mathematical model parameterized using experimental data extant. The model enables determination of age-related changes in AD risk and hippocampal volume, the effects of traumatic brain injury on lifetime AD risk, gene dosage effects, and the effects of spatial variation in $A\beta$ monomer concentrations on millimeter scales. The model is easily interpretable and provides a foundation for development of more comprehensive models of AD development and progression.

All authors contributed to the model development, analysis, and writing of the manuscript.

The authors declare no conflicts of interest.

¹To whom correspondence should be addressed. E-mail: mikel@math.ucla.edu

amount of two forms of the protein, A β 40 and A β 42. A β 42 is only two amino acids longer (42 vs. 40) than A β 40, yet its pathogenicity is substantially higher.

Though A β is produced in the brain throughout life, AD is not usually observed before age 65 (15). AD risk increases exponentially after that, reaching approximately 30% by age 85 (16). Age is the most important risk factor for sporadic AD (17). Apolipoprotein E, which can exist in the body in three different forms, ApoE2, ApoE3, and ApoE4, is a cholesterol carrier protein. The type of apolipoprotein E one expresses also has a significant effect on risk (18) and risk is increased substantially in individuals that express ApoE4 (18). Blunt force trauma to the head, e.g., traumatic brain injury (TBI) or chronic traumatic encephalopathy (CTE), now are understood to be significant risk factors as well (19, 20).

A useful means to understand systems is to model them. Models often are the only way to study complex systems for which determination of the structural and dynamic relationships among elements cannot be accomplished or fully understood experimentally. Deterministic mathematical modelling can be useful in these cases and it has been applied to studying how γ -secretase inhibition affects A β in the CSF and plasma (21); studying microglia, astroglia, and neuron involvements in AD inflammation (22, 23); simulating the effects of drugs in clinical trials (24); relating blood oxygen level-dependent functional magnetic resonance imaging to energy metabolism in the brain (25); describing amyloid processing (26) and prion-like spreading of AD (27); and for other uses as well (28). Model systems for A β structural and conformational studies have been created in silico and provided important insights into factors affecting oligomerization and fibril formation (29). Simulating these processes has been particularly useful for determining how energetics control A β conformation and self-association (30) and for deriving experimentally testable hypotheses about these energetics. One intrinsic problem of in silico simulations is their inability to directly relate natural time steps (sec) with computational time steps (fsec). This creates difficulties when one seeks to understand how A β assembly dynamics relate to the kinetics of disease progression in humans.

Here, we report the creation of a mathematical model of the time-dependence of AD progression and its relationship to the kinetics of A β production, elimination, and toxicity. We find the model predicts biologically significant time scales for development of AD; offers explanations for how blunt force trauma, Down's syndrome, and changes in hippocampal volume affect disease risk; and provides a glimpse into how the disease may spread in the brain.

Assumptions and Model Development

The oligomer cascade hypothesis posits that neuronal death in AD is due to oligomers. In our model, we are therefore interested in describing the coupling between oligomers and loss in neuronal viability. This also requires modelling the kinetics of A β assembly.

We begin by describing the concentration of monomers M , dimers D , and trimers L in the interstitial fluid. As a simplification, once a trimer is formed, it is considered a plaque without dissociation or further growth. This allows for us to concentrate on dimers as representative oligomers and their resulting damage to the cells. We model viable cell density

V as being lost at a rate σ times the dimer concentration as there is not strong evidence of monomers being toxic. At each instant, the percentage change in viable neurons is defined to be γ , what we refer to as the *neuronal death elasticity of AD risk* (similar to the economic concept of "price elasticity of demand," the percent change in demand for each percent increase in price (31)). For kinetics, we stipulate that monomers are produced at a rate S and they are cleared at a rate κ ; dimerization occurs at a rate ν , with a dissociation rate μ ; and trimerization occurs at a rate ζ . To consider the effects of diffusion, we assign monomers a diffusivity \mathcal{D}_M and dimers a diffusivity \mathcal{D}_D . Lastly, there is evidence for rate constants such as S and κ being time dependent with S increasing in time and κ decreasing. When rate time-dependence is considered, we use linear models where λ_S is the time it takes for S to double and λ_κ is the time when κ would reach 0 (at which point the model is no longer accurate). See Figure 1 for a schematic of the mechanisms involved.

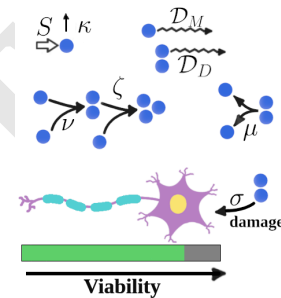


Fig. 1. Model scheme. Monomers are produced at rate S and cleared at a rate κ . Two monomers combine to form a dimer with rate constant ν and a dimer can dissociate at rate μ into two monomers. Monomers and dimers can combine to form trimers at rate ζ , with no backwards reactions present. Trimers are considered plaques. Neurons are killed at a rate σ times the dimer concentration. Thus, as the dimer concentration rises, so does the speed of neuronal death.

Full details of parameter estimation are provided in the Supporting Information. Here, we provide an overview of the steps taken to arrive at the parameters in Table 1. See figure 2 for an illustration. Note that a variable with a bar indicates a representative scale/size for that variable. For instance, monomer production S could be time-dependent and \bar{S} is a representative size of S . From experiments with brain slice cultures and mixed neuron-glia cultures, oligomer toxicity was examined at different concentrations (32, 33), allowing us to estimate $\bar{\sigma}$ from a survival model (34). The loss of neurons is coupled with increased risk of AD through the neuronal death elasticity of AD risk γ , based on the notion that AD develops when one or more neurons (35) critical for memory processes dies. We estimate γ by using AD incidence data. Literature results on A β monomer production rates in single neurons (36) and knowing the density of neuron/glia cells in Rhesus monkeys (37) allow us to estimate \bar{S} . Further studies that show how the activity of β -secretase may increase with age (38–40) allow us to estimate λ_S . Likewise, experiments that show how A β clearance changes with age (38) allow us to estimate $\bar{\kappa}$ and λ_κ . Measured dimer (or soluble A β) concentrations from the literature allow us to estimate the characteristic scale of the dimer concentration (6, 41). Based on some further assumptions relating to the relative speed

Parameter	Meaning	Value
\bar{S}	Baseline monomer production rate	$1.63 \times 10^{-11} \text{ M s}^{-1}$
$\bar{\kappa}$	Baseline monomer loss rate	$6.17 \times 10^{-5} \text{ s}^{-1}$
$\bar{\nu}$	Baseline monomer combination rate	$2.25 \times 10^3 \text{ M}^{-1} \text{ s}^{-1}$
$\bar{\mu}$	Baseline dimer dissociation rate	$7.86 \times 10^1 \text{ s}^{-1}$
$\bar{\zeta}$	Baseline monomer-dimer combination rate	$1.01 \times 10^3 \text{ M}^{-1} \text{ s}^{-1}$
λ_S	Linear growth doubling time of production	$4.85 \times 10^9 \text{ s [154 yr]}$
λ_κ	Linear decay time to zero for clearance	$3.60 \times 10^9 \text{ s [114 yr]}$
\mathcal{D}_M	Monomer diffusivity	$5.47 \times 10^{-7} \text{ cm}^2 \text{ s}^{-1}$
\mathcal{D}_D	Dimer diffusivity	$4.30 \times 10^{-7} \text{ cm}^2 \text{ s}^{-1}$
$\bar{\sigma}$	Baseline cell-dimer damage rate	$4.94 \text{ M}^{-1} \text{ s}^{-1}$
T_D	Survival time after AD diagnosis	$2.23 \times 10^9 \text{ s [7.1 yr]}$
T_L	Life expectancy in United States	$2.48 \times 10^9 \text{ s [78.5 yr]}$
γ	Neuronal death elasticity of AD risk#	6.00×10^{-1}
\bar{L}	Characteristic plaque (trimer) concentration	$6.73 \times 10^{-7} \text{ M}$
\bar{M}	Characteristic monomer concentration	$2.64 \times 10^{-7} \text{ M}$
\bar{D}	Characteristic dimer concentration	$1.00 \times 10^{-12} \text{ M}$
\bar{x}	Characteristic lengthscale#	$9.42 \times 10^{-2} \text{ cm}$
\bar{t}	Characteristic timescale#	$1.62 \times 10^4 \text{ s [4.5 hr]}$

Table 1. Values of parameters for the model. See Figure 2 for an explanation of how these values were determined; Bars (e.g., \bar{S}), indicate a quantity representative of that in a healthy brain; # indicates a scaling that was determined from the model. Note that some of these quantities may vary in time.

of the different reactions and results pertaining to estimated oligomer concentrations when $A\beta$ monomer clearance is impaired (42), we arrive at estimates for the characteristic scale of the monomer concentration, the trimerization rate ζ , dimer dissociation rate $\bar{\mu}$, and dimerization rate $\bar{\nu}$. In modelling prevalence, we consider the number of years a patient survives with AD. As a simplification, we assume that after a course of illness of length $T_D = 7.1$ years, all AD patients die (43). We also estimate lifetime risk by using the average life expectancy in the United States of 78.5 years (44) and computing disease prevalence at that age.

Monomers, Dimers, and Plaques. We denote t as time (age) and M , D , and L as the concentrations of monomers, dimers, and plaques, respectively. The kinetics are modelled by the partial differential equations (PDEs) Eqs. (1)-(2).

$$\frac{\partial M}{\partial t} = S + \mathcal{D}_M \Delta M - \kappa M - \nu M^2 - \zeta MD + 2\mu D \quad [1]$$

$$\frac{\partial D}{\partial t} = \frac{1}{2} \nu M^2 + \mathcal{D}_D \Delta D - \mu D - \zeta MD \quad [2]$$

The plaque concentration is described by Eq. (3)

$$\frac{dL}{dt} = \zeta MD \quad [3]$$

as we assume plaques do not diffuse or dissociate. If only time dynamics are considered without modelling space, Eq. (1) and Eq. (2) are replaced by two ordinary differential equations (ODEs):

$$\frac{dM}{dt} = S - \kappa M - \nu M^2 - \zeta MD + 2\mu D \quad [4]$$

$$\frac{dD}{dt} = \frac{1}{2} \nu M^2 - \mu D - \zeta MD. \quad [5]$$

The symbol Δ represents the Laplacian operator, a type of second partial derivative in space defined as the sum of the second partial derivatives with respect to each Cartesian coordinate direction. It describes diffusive processes and its use in Eqs. (1)-(2) ensures that species will move from regions of higher concentration to regions of lower concentration.

It has been observed that $A\beta$ clearance rate decreases with age (45), whereas the activity of β -secretase increases (38). Many forms could be chosen for $S(t)$ and $\kappa(t)$ for these respective rates at a time t . For $S(t)$ and $\kappa(t)$, we employ linear models using data presented in the Supporting Information to write

$$S(t) = \bar{S}(1 + t/\lambda_S) \quad [6]$$

$$\kappa(t) = \bar{\kappa}(1 - t/\lambda_\kappa). \quad [7]$$

The form of $S(t)$ assumes that monomer production is directly proportional to the activity of β -secretase. It is possible that a combination of genetics and lifestyle factors play a role and may modify the rates that S and κ change. It is also likely the other rates σ , ν , μ , and ζ could vary with age. We note that the model loses validity for $t \geq \lambda_\kappa \approx 114$ yr as that would yield a zero or negative clearance rate.

Cell Viability, Incidence, and Prevalence. Over each small volume of brain tissue, we model the cell viability V in the interval $[0, 1]$ as the number density of viable neuronal cells divided by the number density of neurons in perfectly healthy brain tissue. We model the decrease in this viability with a hazard function which is proportional to the oligomer concentration by

$$\frac{dV}{dt} = -\sigma DV. \quad [8]$$

Viability V decreases faster the more oligomers are present and σ is a coupling constant. Cells with better repair mechanisms will have a smaller σ value, making them less sensitive to the oligomers, whereas a larger σ means the cells die more quickly due to oligomers. In principle, the viability is spatially-dependent, as D could be spatially-dependent. Parameters for such a model are not found in the literature, but we fit for σ using cell viability assay data (32, 33).

As described in the Supporting Information, given the viability model with homogeneous brain tissue, we also identify the survivorship function $H(t)$ (fraction of individuals who do not have AD by age t), incidence $I(t)$ (per capita rate of AD development of age t individuals), prevalence $P(t)$ (fraction of

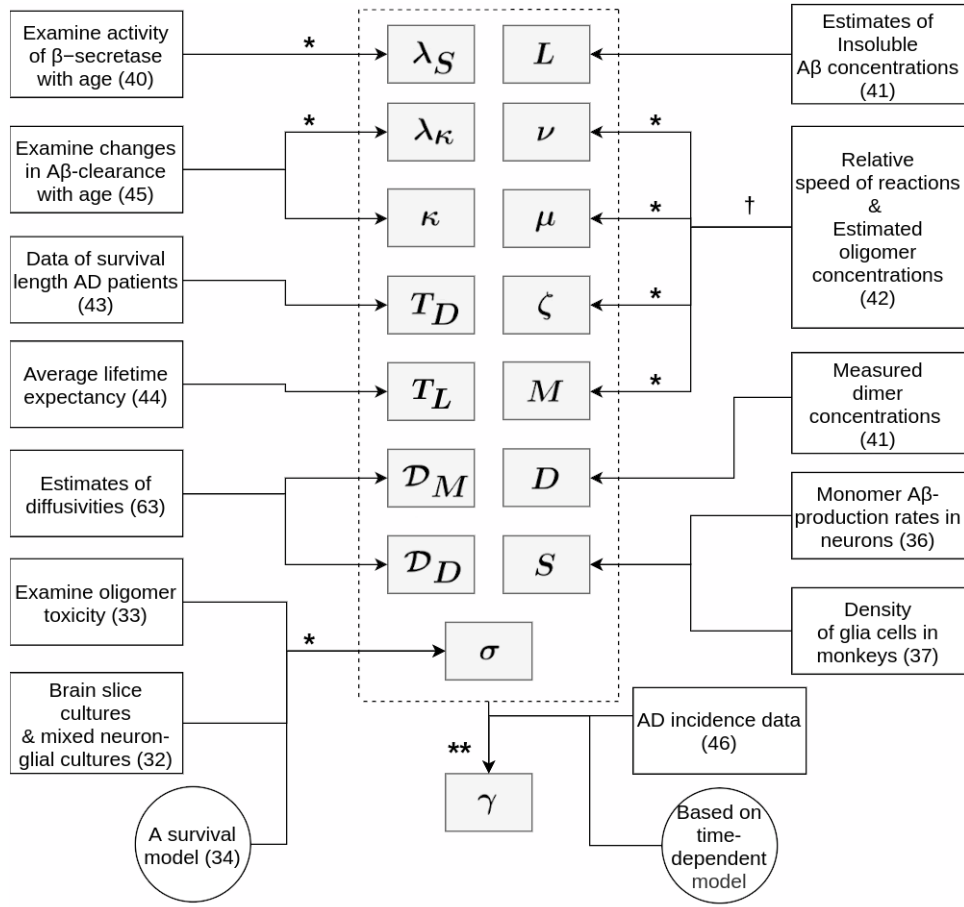


Fig. 2. Means of obtaining model parameters. All model parameter values were obtained from the literature. A † denotes that extra assumptions were required to arrive at the parameter value; * denotes that the values were fitted from existing data in the literature; ** denotes that the parameter was determined from the completed model.

individuals age t with AD), and lifetime risk Υ (prevalence of AD among those of age T_L) through

$$H(t) = V^\gamma \quad [9]$$

$$I(t) = \gamma\sigma D \quad [10]$$

$$P(t) = 1 - \frac{H(t)}{H(t - T_D)} \quad [11]$$

$$\Upsilon = P(T_L), \quad [12]$$

where Eqs. (9)-(11) are valid for $114 \text{ yr} = \lambda_\kappa > t \geq T_D = 7.1 \text{ yr}$. The choice of γ in Table 1 is made by considering AD incidence data.

Solutions. Solving these equations can be complicated. However, in the parameter regime considered, various approximations are possible owing to a separation of time scales. There are fast time scales for dimer loss (centi-seconds), intermediate time scales for monomer decay (hours), and long time scales for changes in kinetic rate constants and loss of neuronal health (decades). The relative sizes of terms can also be exploited. Since the losses due to trimerization are, by model construction, negligible in the dimer evolution, the dimer concentration is controlled by dimerization and dimer dissociation forcing D to scale quadratically with M . This also means the monomer concentration is described through a balance of

production, clearance, and possibly diffusion, which can also be solved analytically. Finally, owing to the slow changes in rate constants, and relatively low toxicity of dimers at their natural concentrations, over the timescales relevant to AD, the monomers and dimers are always quasi-static and the viability V is well-described by a simple decay with instantaneous decay rate being proportional to the present dimer concentration.

Ordinary Differential Equations. With only time-dependence (assuming conditions in the brain are uniform throughout), after the effects of initial conditions are no longer relevant (see Supporting Information), we have

$$M(t) = \frac{S(t)}{\kappa(t)} \quad [13]$$

$$D(t) = \frac{1}{2} \frac{\nu(t)S^2(t)}{\mu(t)\kappa^2(t)} \quad [14]$$

$$L(t) = \int_0^t \frac{\zeta(u)\nu(u)S^3(u)}{2\mu(u)\kappa^3(u)} du \quad [15]$$

$$V(t) = \exp\left(-\int_0^t U(u)du\right) \quad [16]$$

where

$$U(t) = \frac{\sigma(t)\nu(t)S^2(t)}{\mu(t)\kappa^2(t)}. \quad [17]$$

$$M(x) = \frac{\bar{S}}{\bar{\kappa}} + \rho \frac{\bar{S}}{\bar{\kappa}} \begin{cases} \frac{e^{-\sqrt{\frac{\bar{\kappa}}{\mathcal{D}_M}|x|}}}{\sqrt{\frac{\bar{\kappa}}{\mathcal{D}_M}|x|}} \left[\sqrt{\frac{\bar{\kappa}}{\mathcal{D}_M}|x|} \cosh\left(\sqrt{\frac{\bar{\kappa}}{\mathcal{D}_M}|x|}\right) - \sinh\left(\sqrt{\frac{\bar{\kappa}}{\mathcal{D}_M}|x|}\right) \right] \\ + \frac{\sinh\left(\sqrt{\frac{\bar{\kappa}}{\mathcal{D}_M}|x|}\right)}{\sqrt{\frac{\bar{\kappa}}{\mathcal{D}_M}|x|}} \left[\sqrt{\frac{\bar{\kappa}}{\mathcal{D}_M}} \left(|x|e^{-\sqrt{\frac{\bar{\kappa}}{\mathcal{D}_M}|x|}} - X^*e^{-\sqrt{\frac{\bar{\kappa}}{\mathcal{D}_M}X^*}} \right) - e^{-\sqrt{\frac{\bar{\kappa}}{\mathcal{D}_M}X^*}} + e^{-\sqrt{\frac{\bar{\kappa}}{\mathcal{D}_M}|x|}} \right], & |x| < X^* \\ \frac{e^{-\sqrt{\frac{\bar{\kappa}}{\mathcal{D}_M}|x|}}}{\sqrt{\frac{\bar{\kappa}}{\mathcal{D}_M}|x|}} \left[\sqrt{\frac{\bar{\kappa}}{\mathcal{D}_M}} X^* \cosh\left(\sqrt{\frac{\bar{\kappa}}{\mathcal{D}_M}X^*}\right) - \sinh\left(\sqrt{\frac{\bar{\kappa}}{\mathcal{D}_M}X^*}\right) \right], & |x| \geq X^* \end{cases}, \quad [23]$$

$$D(x) = \frac{\bar{\nu}M(x)^2}{2\bar{\mu}} \quad [24]$$

$$L(x, t) = \frac{\bar{\zeta}\bar{\nu}M(x)^3}{2\bar{\mu}} t \quad [25]$$

$$V(x, t) = \exp\left(-\frac{\bar{\sigma}\bar{\nu}M(x)^2}{2\bar{\mu}} t\right). \quad [26]$$

From Eq. (14) and Eq. (16), we obtain the incidence and prevalence of the disease with Eq. (10) and Eq. (11). In the special case that $S, \kappa, \mu, \nu, \zeta, \sigma$ are constant, these become

$$M = \frac{\bar{S}}{\bar{\kappa}} \quad D = \frac{1}{2} \frac{\bar{\nu}\bar{S}^2}{\bar{\mu}\bar{\kappa}^2} \quad [18]$$

$$L(t) = \frac{\bar{\zeta}\bar{\nu}\bar{S}^3}{2\bar{\mu}\bar{\kappa}^3} t \quad V(t) = \exp(-\bar{U}t) \quad [19]$$

$$H(t) = \exp(-\gamma\bar{U}t) \quad I(t) = \gamma\bar{U} \quad [20]$$

$$P(t) = 1 - \exp(-\gamma\bar{U}T_D) \quad \Upsilon = 1 - \exp(-\gamma\bar{U}T_D), \quad [21]$$

where the quantity

$$\bar{U} = \frac{\bar{\sigma}\bar{\nu}\bar{S}^2}{2\bar{\mu}\bar{\kappa}^2}. \quad [22]$$

The value \bar{U} gives a baseline estimate for the rate neuronal viability is lost in healthy brain tissue.

Partial Differential Equations. To study spatial effects, we consider the question of a localized excess of $A\beta$ monomers and how this affects cells in the vicinity. We consider a *spherically symmetric* source of excess monomers. We consider a hypothetical scenario with $\kappa = \bar{\kappa}, \mu = \bar{\mu}, \nu = \bar{\nu}, \zeta = \bar{\zeta}$, and $\sigma = \bar{\sigma}$. We choose $S = \bar{S}$ except over a sphere of radius $X^* = 2\bar{x}$ centered at $x = 0$ where the monomer production is increased by $\rho = 22.8\%$. There, $S = \bar{S}(1 + \rho)$. The choice of X^* is made so as to be on the order of \bar{x} , a characteristic length a monomer may diffuse before its clearance; and the choice of ρ comes from our findings on traumatic brain injury where $0.228\bar{S}$ is a representative increase in monomer production. We wish to study how the $A\beta$ assemblies vary in space and how the viability changes over space and time. The solutions are presented in Eqs. (23)-(26).

Model Predictions

From the model developed, a series of comparisons can be made between our model and clinical observations. In general, we can consider our ODE model in two forms:

- a **static model** where all rate constants are constant over a lifetime
- a **dynamic model** where the rate constants S and κ vary as in Eqs. (6)-(7).

While we believe the dynamic model is more accurate, more explicitly taking into account the aging process, it does not always lend itself to simple analysis and further assumptions may be required. In such cases, we use the static model. We note that the static model still involves time-dependent changes in the brain physiology and the rate constants are representative estimates; it simply does not include time-dependent S and κ rates.

Our PDE model, which takes into account spatial variations in the system, is done with the kinetic rate constants being constant in time.

AD Incidence and Prevalence.

Clinical Data. Age is the single leading risk factor for developing AD. In the ODE model, we can compare the predicted incidence and prevalence from the model with the clinical data. We consider the incidence rate (per person) in the United States (46) and the AD prevalence by age range in the World Health Organization region AMRO A (16). We investigate these data with the ODE model.

Model. The incidence and prevalence described here are given by Eqs. (10), (11), (20)₂, and (21)₁.

Static Model (κ, S constant): Over a lifetime, the incidence would be a constant, \bar{I} , given by

$$\bar{I} = \bar{U}\gamma = 9.34 \times 10^{-5} \text{ yr}^{-1}.$$

By Taylor expanding Eq. (21)₁, the prevalence at each age is approximately constant, \bar{P} , with value

$$\bar{P} = \bar{U}\gamma T_D = 0.0663\%,$$

where γ is chosen based on the dynamic model below.

Dynamic Model (κ, S time-dependent): Allowing the rates to vary, we can examine how the incidence and prevalence increase with age, which we depict in Figure 3. We choose γ so that the dynamic model incidence at age 60 matches clinical data, finding $\gamma = 0.600$. Using a linear best fit on the log-scale, our dynamic model predicts doubling times for prevalence and incidence of 12 y and 11 y, respectively. The fact that the model's predictions are within a factor of 2–3 of the clinically observed times is encouraging. If other rate constants also changed over time, it could be possible to match the data.

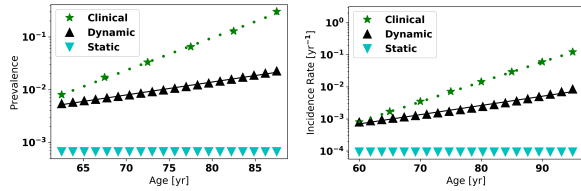


Fig. 3. Incidence and prevalence. Comparison of static and dynamic models with clinical data for AD. The dotted green lines represent the line of best fit to clinical data on log-scale; The black solid lines are the lines of best fit to the dynamic model on log-scale. For prevalence, the clinical doubling time is 4.9 y and our dynamic model predicts 12 y. For incidence, the clinical doubling time is 4.9 y and our dynamic model predicts 11 y. The value γ is chosen so that clinical and dynamic model incidence agree at age 60.

We can also compute lifetime risk for AD in our model. It has been reported that among those age 75–79, the prevalence of AD is $6.5 \pm 0.5\%$ (SD) (16), which would include prevalence among those age $T_L = 78.5$ y and what we define as lifetime risk. The results we compute from Eq. (12) are 0.0663% and 1.24% for the static and dynamic models, respectively.

Gene Dosage and Down’s Syndrome.

Clinical Data. Due to the under- or over-expression of particular genes, the production of monomers could be altered. For individuals with Down’s Syndrome, the trisomy of chromosome 21 results in life-long levels of $A\beta$ production that are ≈ 1.5 times that of normal individuals and an AD incidence at least 3 times higher (47). In addition, Down’s Syndrome patients may present symptoms of dementia as early as age 40 (48).

Model. In the ODE model, we can investigate the effect of increasing the monomer production rate $S(t)$ by 50%. In this case, both the incidence rate and the prevalence of AD would increase by a factor of 2.25, which is close to the ≥ 3 increased relative risk for AD noted for Down’s Syndrome. More generally, through gene dosage, if the monomer production rate were to change by a factor ω , the incidence and prevalence should scale by ω^2 .

Hippocampal Volume (HV).

Clinical Data. Changes in HV can take place during the aging process but these changes are particularly extensive in AD patients. Frankó et al. used MRI to estimate HV in longitudinal studies of AD patients, mean age 75, patients with mild cognitive impairment (MCI), mean age 75, and controls, mean age 76. They found that HV decreased by 42 mm^3 , 30 mm^3 , and 15 mm^3 per year in the AD, MCI, and control groups, respectively. The average HVs reported at initial scans were 3934 mm^3 , 4127 mm^3 , and 4464 mm^3 , respectively. Using these data, we can estimate that around age 75, the three groups have annual decreases in HV of 1.06% (AD), 0.727% (MCI), and 0.336% (control). We note some studies in cognitively normal individuals have failed to find significant differences in HV but did find statistically significant differences in some brain measures like the thicknesses of the entorhinal cortex and parahippocampal gyrus when subjects were classified into two groups $A\beta^+$ and $A\beta^-$ with a Pittsburg Compound B (PiB) MRI scan (49). In a study by Gordon et al. (50), participants received MRI and PiB/PET scans along with assays of tau and phosphorylated

tau. Patients then were classified into four disease states reflecting the presence/absence of amyloid ($A\beta^+/A\beta^-$) and the presence/absence of CSF tau/phosphotau, which were used as a proxy for neurodegeneration (ND^+/ND^-). We focus here on the states 0 ($A\beta^-/ND^-$) and 2 ($A\beta^+/ND^+$), which we consider normal or “AD.” The study found those in state 0 (mean age 63.4) had measured HVs of 7755 mm^3 and those in state 2 (mean age 71.6) had measured HVs of 7063 mm^3 . Thus, the AD patients of mean age 71.6 had HVs that were only 91.1% as large as those without AD and mean age 63.4.

Model. In the ODE model, if we assume HV is proportional to $V(t)$, the model yields estimates for HV changes over time. We test our static and dynamic models against the data described above. We find the dynamic model adequately describes cognitively normal individuals. To describe the HV rate of change in AD patients and the HV ratios at different ages, we need to scale $U(t)$ (Eq. (17)) up by a factor $F > 1$. This then leads us to examine how a distribution of rate parameters within the population could influence clinical outcomes. We examine this in the more tractable static model.

Static Model (κ, S constant): With static values, each year, the hippocampal volume should decrease by a rate

$$\frac{-V'(t)}{V(t)} = \bar{U} = 0.0154\%y^{-1}.$$

This is a factor of ≈ 22 smaller than the typical loss of HV in non-AD patients.

Dynamic Model (κ, S time-dependent): We compare the model predictions with clinical findings in Figure 4. We plot what the HV would look like with the dynamic model with the relative change ($V'(t)/V(t) = -0.29\%/y$) at age $t = 75$ y. This agrees well (within $\approx 16\%$) with the rate of change of $-0.336\%/y$ in the control group of Frankó.

Our model is attempting to describe the average patient and their resulting HV (or neuronal viability) over a lifetime. AD development is seen as a probabilistic event where the probability of having AD depends on the amount of HV lost. Our dynamic model does not match the observed rate of $-1.06\%/y$ for the HVs in the Frankó AD patients (it is off by a factor of ≈ 3.63). One possible means of reconciling this is by assuming the measured AD-pathology stems from a constant rescaling of the rate constants, i.e., $U(t)$ is larger by a factor $F = 3.63$, so as to match $-1.06\%/y$. This **AD-pathology model** with rescaled rate constants is also shown in Figure 4.

Given the dynamic model and the AD pathology model, we can compute the ratio in HVs between those at age 71.6 years (state 2^+) to those of 63.4 years (controls). Taking the HV ratio of our AD pathology model at age 71.6 to the dynamic model at age 63.4 yields 0.859, which is close to the observed 0.911 ratio. We thus speculate that larger values of $U(t)$, the instantaneous rate of neuronal death (see Eq. (17)), are more closely associated with AD.

Distributions of \bar{U} values: We now ask whether the model allows for those with AD to have higher values of $U(t)$ or \bar{U} than the rest of the population. For simplicity, we study the static model and assume $\bar{U} \sim g(u)$ has a probability density function with mean value U^* and standard deviation Σ^* .

On one hand, it may seem obvious that if someone has AD, more neurons have been destroyed and an appreciably

above average \bar{U} is expected (\bar{U} describes the rate of neuronal death). But even people with lower values of \bar{U} can develop AD and there are more people with average or below-average \bar{U} 's than those with \bar{U} 's that are above the average. Thus, is not immediately obvious that AD patients will have above-average \bar{U} values. This above-average \bar{U} in the AD group turns out to be true, however, which we show in the Supporting Information. In particular, the mean value of \bar{U} within the AD population is given by

$$\langle \bar{U} \rangle_{AD+} \approx U^* + \frac{\Sigma^{*2}}{U^*}, \quad [27]$$

and the mean value of \bar{U} within the non-AD population is given by

$$\langle \bar{U} \rangle_{AD-} \approx U^*. \quad [28]$$

Thus, those without AD on average have a “normal” \bar{U} but those with AD on average have an above average \bar{U} . This would allow for consistency between our model and the requirement to scale $U(t)$ to match AD-specific data.

Assuming the F obtained from the dynamic model can be applied to the static model, we can be very specific with Eq. (27) about how spread out \bar{U} -values are within the population. We find that $\frac{\Sigma^{*2}}{\bar{U}^{*2}} = F - 1$ is most consistent with the data. Numerically, with $F = 3.63$, we find that the standard deviation to mean ratio $\Sigma^*/U^* \approx 1.62$.

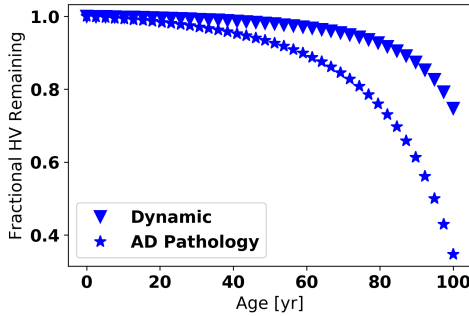


Fig. 4. Hippocampal volume. Time dependence of HV for the dynamic model with or without additional AD pathology. An HV of 1 is maximal. At age 75, the annual changes in hippocampal volume are -0.015% (static model, not shown), -0.29% (dynamic model), and -1.1% (AD pathology model - rates have been scaled to match this value). The HV ratio between those at age 71.6 (AD pathology) to age 63.4 (CN) is 0.859. We can also compare *within models*. The hippocampal volume ratios between age 71.6 to age 63.4 years are as follows: 0.999 (static), 0.984 (dynamic), and 0.944 (AD pathology).

Blunt Force Trauma.

Clinical Data. Whether the risk of developing AD definitively increases as a result of Traumatic Brain Injury (TBI) is not clear (51) as there are many factors at work: the nature of the trauma, its location, whether consciousness was lost, and whether TBI incidents are reported/remembered, etc. However, a more recent study by Fann et al. (52) does provide data for estimated hazard ratios of developing AD given a patient’s history of TBI and years since their first TBI. For our study, we focus upon the long term risk of AD given the number of TBIs using their “model 1”, which adjusts for age, sex, marital status, and calendar period, but does not adjust for other comorbidities

since the comorbidities may reflect physiological differences between individuals that requires further modelling.

After an acute TBI, it has been noted that APP processing increases, resulting in increased $A\beta$ production and deposition (53). In studies on pigs with a head rotational acceleration injury, axonal damage, resulting in an accumulation of APP, has been noted 6 months after injury (54). In humans, axonal damage and intra-axonal $A\beta$ accumulation can last for years (54). It should be noted that neprilysin, an $A\beta$ degrading enzyme, also appears to be upregulated following TBI, which could counteract increased $A\beta$ production.

Model. For simplicity in the ODE model, for each TBI, we assume the monomeric production rate S increases by a fixed amount A , without mitigating effects, and we work with the static model to avoid needing the age of a patient at each of their TBIs.

Assuming that for each TBI, the monomer production rate rises by a constant value, the relative risk (relative to having no TBIs) after having n TBIs should be

$$R = (1 + n \frac{A}{\bar{S}})^2.$$

This sort of model has one free parameter, $a = A/\bar{S}$. In comparing it to a naive, purely linear model where the relative risk is $1 + mn$ for a constant m , the model does much better, as seen in Figure 5. We thus venture the idea that, very approximately, each TBI results in a long-term increase in the monomer production rate of approximately $0.228\bar{S}$.

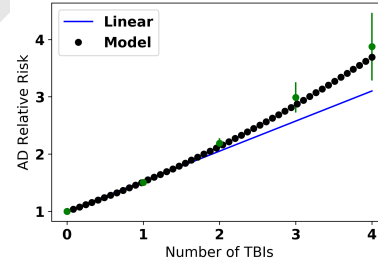


Fig. 5. Traumatic Brain Injury. Two fits for the relative risk R vs number of TBIs, n . Linear fit: $R(n) = 1 + mn$ with m to be fit. Model fit: $R(n) = (1 + an)^2$ with $a = A/\bar{S}$ to be fit. The fitted values are $m = 0.520$ and $a = 0.228$. The respective AIC values (55) are -2.04 and -9.07 . Both visually and through the AIC values, the model significantly outperforms the naive fit.

Spatial Spreading of AD. Using the PDE model, we gain insight into the effects of localized excesses of monomers. In an idealized, spherically symmetric geometry with constant rate constants, we consider a hypothetical scenario. We imagine that over a radius of $2\bar{x}$, the monomer production is increased by an amount $0.228\bar{S}$, the characteristic increase due to a TBI. This results in a modest excess of monomers and dimers above their baseline values. In turn, this affects the viability of cells in that vicinity so that over a lifetime, cell damage is more pronounced nearer to the excess monomer production. We display the results in Figure 6. These results suggest that if a part of the brain is damaged, resulting in a local excess of monomers, the closer that region of damage is to neurons that are particularly important for memory, the more likely lifetime risk may be permanently elevated, even if these neurons were not originally damaged.

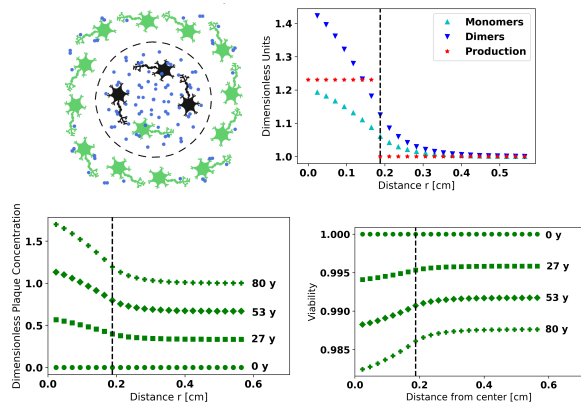


Fig. 6. Spatial model. *Top left:* the excess monomer production is taken to be spherically symmetric. The distance (x -axis) denotes the distance from the center of the source. The dashed circle/lines represent the boundary where excess monomer production ceases. *Top right:* monomer and dimer concentrations, and monomer production rate, versus distance from center. These values have been nondimensionalized by \bar{M} , \bar{D} , and \bar{S} , respectively. *Bottom left:* accumulation of plaques at various ages plotted against position. The concentration has been nondimensionalized by \bar{L} . *Bottom right:* viability at various ages plotted against position.

Discussion

We have developed a mathematical model for AD risk and progression based on the kinetics of $A\beta$ oligomerization and clearance and its relationship to neuronal viability. The model predicts a doubling time for AD risk of ≈ 11 -12 years; reveals that if gene dosage-mediated increases in $A\beta$ monomer production scale by a factor ω , then prevalence is scaled by ω^2 ; predicts age-related HV decreases and through these HV changes gives understanding of possible distributions of \bar{U} (or $U(t)$) within the population; models the effect of blunt force trauma as an increase of monomer production of approximately $0.228\bar{S}$, which yields a value for increased lifetime risk of AD; and, with a simple spatial model of the brain parenchyma, demonstrates a direct relationship between the proximity of neurons to points of increased $A\beta$ monomer production and increased neuronal death rate.

Many of these predictions are consistent with clinical observations. Notably, the ODE model does well at describing disease prevalence and incidence. If the model's rate constants accurately represent those occurring in vivo then, by Eq. (22), the model predicts that the rate of neuronal death (and AD incidence) is proportional to S^2 (S is the $A\beta$ monomer production rate), ν (dimerization rate), and σ (cell sensitivity to dimers); and inversely proportional to both κ^2 (κ is the $A\beta$ monomer clearance rate) and μ (dimer dissociation rate). The quadratic dependencies are most significant: If S increases by a factor of 2 (or if κ decreases by a factor of 2), the neuronal death rate quadruples. *Treatments that lower monomer production or increase monomer clearance thus would be predicted be most beneficial.* The other factors only influence the death rate in direct proportion (or inverse proportion) to their value. For instance, if μ doubles, the death rate goes down by a factor of 2. The ODE model also accounts for the loss of hippocampal volume over a lifetime and the changes in AD risk associated with APP gene dosage. If APP gene expression changes by a factor ω then relative risk scales by ω^2 . This is consistent

with data on Down's Syndrome, where our model predicts a relative risk of 2.25 and clinical observation shows the relative risk is at least 3-fold. The ODE static model also allows us to accurately describe how TBI increases one's lifetime risk of AD if each TBI increases the monomer production rate by $0.228\bar{S}$. The PDE model provides an understanding of how $A\beta$ concentrations and cell viability could vary over millimeter scales, leading us to speculate that the location of a TBI may influence the increased lifetime risk of AD. In particular, even if a brain injury occurs away from a neuron that is especially important for memory, our model suggests that the closer the injury is to such a neuron, the greater the long-term risk of AD.

We emphasize that the goal of our work was to create a simple model that could be modified in the future to account for a greater number of factors contributing to AD etiology and pathogenesis. This would increase the model's sophistication and provide a more accurate representation of the kinetics of disease development. However, the results we have at present are already encouraging. We suggest now a number of modifications that could further improve the models. These improvements include accounting for: (1) the myriad of enzymes involved in $A\beta$ metabolism; (2) genetic factors; (3) heterogeneity in brain structure (no two brains are the same); (4) cell repair; (5) coupling monomer production rates with the health/viability of the cells; (6) distinguishing the unique contributions of $A\beta_{40}$ and $A\beta_{42}$ to the pathogenesis of AD (both were considered together); (7) expanding anatomical considerations from just interstitial fluid to the brain parenchyma and its distinct regions (ideally accounting for stereotypical spreading of disease (Braak staging)); (8) accounting for differences in $A\beta$ -induced toxicity among different neuronal cell types and brain regions; and (9) including contributions of glial cells and microglia to disease pathogenesis.

We also would like to include more data to enable a better accounting for nonlinearities in model results. As a heuristic example, we found roughly that with static rate constants, the hippocampal volume of a subject of age t would scale with $e^{-U t}$. Most studies had a distribution of subject ages and HVs. For our models, we used the mean age for t as the time variable and the mean HV as a target volume as we did not have access to each subject's data. However, *it is not generally true that the mean value of a nonlinear function evaluated at a series of inputs is equal to the nonlinear function evaluated at the mean value of the inputs.*

Most of our results come from the ODE model, which describes the brain as a homogeneous volume or describes the case in which the diffusion of monomers and dimers is infinite. The PDE model offers more opportunity to explore spatial effects. While our present PDE analysis did not consider the finiteness of the brain, the model could be adapted to describe boundary conditions such as the blood brain barrier and differences in brain compartments such as location-dependent rate constants, varying diffusivities, etc.

In many cases, the model's limitations stem from a lack of data within the scientific community pertaining to in vivo measurements of $A\beta$ kinetics and neuronal toxicity of oligomers. It would be of particular interest if the modeling assumptions and assumed rate constants could be validated clinically. However, one of the benefits of such a simple model is that many results can be obtained and understood from simple formulae, which

could easily become intractable, and inaccurate (overfitted), with more elements and systems included. We expect many of the results presented would still hold, even if the rate constants changed over one or two orders of magnitude—provided the same processes can be deemed negligible from the larger-scale system behavior. In this sense, the model is quite robust even considering its limitations.

There are numerous other factors that have been implicated in AD risk and pathogenesis. Among these are lifestyle factors such as diet, exercise, mood, brain activity, education, and sleep quality (impaired glymphatic clearance of A β monomers during sleep (56, 57) may reduce κ , which would accelerate neuronal damage). Of course, many other factors likely exist about which we are unaware. These also could influence the model's rate parameters so that some individual's exhibit a faster neuronal death rate and increased risk for AD at every age.

Conclusions and Future Work

We have developed a simple mathematical model describing the time dependence of development of AD and the contributions of A β monomers, dimers, and trimers to it. The model produces explicit equations whose solutions are consistent with clinical features of disease development and allow for interpretation of individual terms and rate constants. For example, the ratio of monomer production to monomer clearance, S/κ , is a term that is highly significant, suggesting that its reduction would lessen disease risk and slow progression. The model serves as a starting point for numerical simulations and in silico studies. Most importantly, the fact that such a complicated disease process can be simplified so much and produce accurate, clinically verified predictions suggests that the model can be used to test existing, and yield new, hypotheses about disease causation. This would be especially valuable for studying aspects of AD for which little experimental data are available or the application of experimental or clinical methods of study is impractical. For example, the model could be used to explore the effects of predetermined numbers and magnitudes of TBIs on localized increased expression of APP and A β and consequent disease initiation and progression.

ACKNOWLEDGMENTS. The authors would like to thank Colleen Sun for help in the early stages of this research and acknowledge grant support provided by the State of California, Department of Public Health, Alzheimer's Disease Program (#16-10322 (DBT)).

Supporting Information: Parameter Estimation

We present our analyses to estimate the model parameters. In general, we seek to estimate parameters that are representative (perhaps within an order of magnitude) of a healthy brain. Variations in these parameters, which our model studies, could lead to disease.

Viability Modelling. One important metric for brain health is cell viability, which we denote $V(t)$ and define to be the number of viable neurons per unit volume, *relative to the optimal value in a healthy brain with no neuronal death*. Through aging and various insults, the value of V will decrease. We let D represent the concentration of dimers. For a given neuron, we denote $T > 0$ to be its age when it dies. We use survival analysis and hazard functions to model this (34).

Over a short time window δt , we assume

$$\Pr(t < T \leq t + \delta t) | T \geq t = \sigma D \delta t$$

for some $\sigma > 0$. In other words, given that a cell lives as long as time t , the probability it dies over the next interval of length δt is

Oligomer Concentration [M]	Survival Fraction	Standard Error	Source
0	1	0.0256	Lambert
5×10^{-9}	0.862	0.0684	Lambert
5×10^{-8}	0.822	0.0649	Lambert
5×10^{-7}	0.806	0.0572	Lambert
5×10^{-6}	0.729	0.0890	Lambert
0	1	0.0598	Cizas
2.5×10^{-7}	1	0.0762	Cizas
5×10^{-7}	0.849	0.0918	Cizas
1×10^{-6}	0.275	0.0975	Cizas
2×10^{-6}	0.120	0.106	Cizas

Table 2. Viability Data. Data are based on work by Lambert et al. (32) and Cizas et al. (33). The values were estimated from graphs published in the cited works. Standard errors for the Lambert data in the control (oligomer concentration of 0) are based on a worst-case estimate. The figure markings obscured the errorbars and we chose the half-width of the largest marker as the standard error as part of the calculation. The study of Lambert et al. did not specify whether the errorbars displayed were standard errors or standard deviations. We assume standard error. Such variations only change σ by a modest scaling factor.

proportional to δt (and to the oligomer concentration). Alternatively we can think that the event of cell death is instantaneously a Poisson (memoryless) process with rate σD . As a differential equation, we have

$$\frac{dV}{dt} = -\sigma DV. \quad [29]$$

To estimate σ , we choose two experiments (32, 33) from the literature studying oligomer toxicity on neurons. There are many papers that study this phenomena, but many study neuron cultures in isolation or at higher than biologically representative oligomeric concentrations. The Lambert paper measured cell death on mouse brain slice cultures subjected to various levels of oligomers for 24 hours; and the Cizas paper measured cell survival in mixed neuronal-glial cell cultures subjected to various levels of oligomers for 24 hours. For our fitting, we assume:

- The cell viability V begins at maximum $V = 1$.
- The experiments directly measure V (in expectation, the fraction of surviving cells should indeed be V).
- General oligomer toxicity and dimer toxicity are the same.
- The value σ does not vary over the duration of the experiment.
- The only observable processes taking place are cell death due to the oligomers and thus at time t we have $V(t) = \exp(-\sigma D t)$.

After estimating values from their respective published graphs, converting cell death to cell survival in Lambert, and normalizing both datasets by the survival of their respective controls (see Table 2), we fit for σ in Eq. (29) with a Maximum Likelihood estimate (58). See Figure 7. We obtain $\bar{\sigma} = 4.9 \pm 0.4 \text{ M}^{-1} \text{ s}^{-1}$ (SD) to be the characteristic size of the dimer toxicity.

In order to provide the survival fractions of table 2, we divided the survival rates from the experiments by their respective controls and added errors in quadrature to report the standard errors.

As a remark: we could allow V to be spatially dependent as well due to D potentially varying in space. Equation Eq. (29) would be unchanged, however, i.e. there would not be any explicit spatial-dependence and all spatial variation would be implicit through the varying concentration of dimers.

Incidence and Prevalence. For this modelling, we assume the brain tissue of interest (such as the hippocampus) has a uniform distribution of monomers and oligomers and a uniform viability measure $V(t)$. We begin by considering $H(t)$, the “survivorship function,”

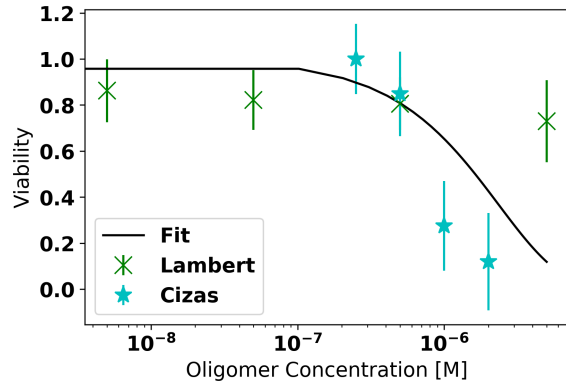


Fig. 7. Viabilities at various oligomer concentrations after 24 hours. We fit the model to viability data. The errors bars represent two standard errors.

being the “healthy” fraction of the population still alive at age t that does not have AD. We have

$$H(t) = \Pr(\text{AD has not developed by age } t | \text{alive at age } t).$$

We again use a survival analysis. Over a short time interval δt , we assume

$$\Pr(\text{AD develops in } (t, t + \delta t] | \text{no AD up to time } t) = \gamma \frac{V(t) - V(t + \delta t)}{V(t)},$$

i.e., the probability someone develops AD in the interval $(t, t + \delta t]$ if they did not have it up to time t is proportional to the percentage of remaining neurons lost over the interval $(t, t + \delta t]$, where $\gamma > 0$ is a dimensionless proportionality constant that we expect to be on the order of unity. This is motivated by the fact that just a small number of neurons may be highly influential in memory formation (35) and we are describing the probability one of these influential neurons dies over the interval of width δt . In expectation, and with infinitesimal time steps,

$$\frac{dH}{H} = \gamma \frac{dV}{V}.$$

With $H(0) = 1$ and $V(0) = 1$, the solution is that

$$H(t) = V(t)^\gamma.$$

To model prevalence, we note that Alzheimer’s patients live, on average, $T_D = 7.1$ years after diagnosis. Without specifically modelling the factors that lead to mortality, we assume that all Alzheimer’s patients die after T_D years since being diagnosed. This factor is relevant in computing the prevalence, $P(t)$, which should be the fraction of the population (AD and non-AD) still alive at age t that has AD. This can be expressed as

$$P(t) = \frac{H(t - T_D) - H(t)}{H(t - T_D)}.$$

Neglecting the edge case of $t < T_D$, the numerator is the fraction of patients with AD within the population who are still alive at time t (they cannot be diagnosed earlier than $t - T_D$). The denominator is all people still alive, with and without Alzheimer’s disease (to still be alive, they must develop AD later than $t - T_D$). The incidence (fractional rate people are diagnosed per unit time), $-H'(t)/H(t)$, is

$$I(t) = \gamma \sigma D.$$

Monomer, Dimer, and Plaque Concentrations. We denote parameters of interest with a bar to indicate a characteristic value in a healthy brain.

Monomer Production Rate \bar{S} : To obtain an estimate for \bar{S} , we use that the density of neuron/glia cells in the hippocampi of Rhesus monkeys is $7 \times 10^4 - 1.1 \times 10^5 \text{ mm}^{-3}$ (37) (we use a value of $9 \times 10^4 \text{ mm}^{-3}$) and that 2–4 monomers are released per cell per second in rat neurons (36) (we use 3), to arrive at the value of $\bar{S} = 1.63 \times 10^{-11} \text{ M s}^{-1}$.

It has also been found that through the aging process, β -secretase increases in activity (38). And in AD patients the increase in β -secretase could be 63% higher than controls (39). Authors have attempted to measure the increase in β -secretase activity with age and from the data it appears it increases by approximately 65% over 100 years (40). These authors also found that β -secretase activity increases by 58% over 50 years in Down’s Syndrome patients and that α -secretase appears to stay about the same throughout life for those with and without Down’s Syndrome. We assume that monomer production rate is linearly proportional to this β -secretase activity.

Monomer Clearance Rate $\bar{\kappa}$: $A\beta$ monomers are cleared at a rate $\kappa = 5.07 \times 10^{-5} \text{ s}^{-1}$ for subjects of age 30 and $2.05 \times 10^{-5} \text{ s}^{-1}$ for subjects of age 80 (45). We assume a linear decay in κ throughout life.

Dimer Concentration \bar{D} : Shankar et al. found $A\beta$ -dimer concentrations in the range of 0.04–1.44 nM (6) in AD brains. We use the geometric mean of 0.24 nM as a representative AD dimer concentration from the Shankar study. From Lue et al., the range of total soluble $A\beta$ was measured to be 0 + 1.9 pg/g (healthy $A\beta$ -42 + $A\beta$ -40) or 15.5 + 66.5 pg/g (AD $A\beta$ -42 + $A\beta$ -40) in the endorhinal cortex of humans (41). With $A\beta$ -42 having a molar mass of 4514 g/mol and $A\beta$ -40 having a molar mass of 4329.9 g/mol, and assuming brain tissue has a density of approximately 1 g/cm³, this places the Lue data as $2.19 \times 10^{-13} \text{ M}$ (healthy) and $9.16 \times 10^{-12} \text{ M}$ (AD) of dimers. For a model value, we choose $\bar{D} = 1 \text{ pM}$, which is more on the scale of the Lue study.

Insoluble $A\beta$ -concentration: From the Lue et al. study (41), we can estimate the concentration of insoluble $A\beta$ that accumulates in the brain over a lifetime (roughly 80 years). The non-AD patients and AD patients had insoluble $A\beta$ concentrations of $2.02 \times 10^{-6} \text{ M}$ and $3.84 \times 10^{-5} \text{ M}$, respectively. These concentrations reflect the number of *monomers present*. A representative scale for the plaques is chosen as $\bar{L} = 6.73 \times 10^{-7} \text{ M}$ (recall we model trimers as being plaques).

Extra Assumptions. In order to estimate more parameters, we make a series of assumptions:

1. the monomers and dimers are in fast equilibrium so the contribution so that conversions from monomers to dimers and dimers to monomers are balanced in describing the monomer concentration;
2. the loss of monomers to forming higher order structures is negligible in comparison to the loss due to clearance so that in combination with the previous assumption, $\bar{M} = \bar{S}/\bar{\kappa}$;
3. the rate dimers combine with monomers to form higher order structures $\zeta \bar{M} \bar{D}$ is approximately $2.76 \times 10^{-16} \text{ M s}^{-1}$ by assuming the accumulation of insoluble $A\beta$ in healthy patients in the Lue study is constant over 80 years;
4. the loss of dimers to forming higher order structures is negligible in comparison to the loss of dimers due to dissociation: $\zeta \bar{M} \bar{D} \ll \bar{\mu} \bar{D}$;
5. dimer dissociation into monomers greatly exceeds dimer production from monomers so that $\frac{1}{2} \bar{\nu} \bar{M}^2 \ll \bar{\mu} \bar{D}$ (this is consistent with the dimer concentration being much smaller than the monomer concentration (59)) and combined with the previous assumption we have $\bar{D} \approx \frac{\bar{\nu} \bar{M}^2}{2 \bar{\mu}}$;

Monomer Concentration \bar{M} : From assumptions 1 and 2, we deduce $\bar{M} = \bar{S}/\bar{\kappa} = 3.21 \times 10^{-7} \text{ M}$.

Monomer-Dimer Combination Rate $\bar{\zeta}$: From assumption 3, we compute $\bar{\zeta} = 860 \text{ M}^{-1} \text{ s}^{-1}$.

Ratio of Monomer-Monomer Combination to Dimer Dissociation Rates $\varrho = \bar{\nu}/\bar{\mu}$: By assumptions 4 and 5, we have that $\bar{\nu}/\bar{\mu} = 19.3 \text{ M}^{-1}$.

Dimer Dissociation Rate $\bar{\mu}$: By disrupting $A\beta$ -clearance, the synaptotoxic peptide concentration can build up to 50–500 nM (42). By setting $\bar{\kappa}$ to zero and looking for equilibrium concentrations of the monomers M_c and dimers D_c , we find they satisfy

$$\begin{aligned} \bar{S} - \varrho\bar{\mu}M_c^2 - \bar{\zeta}M_cD_c + 2\bar{\mu}D_c &= 0 \\ \frac{1}{2}\varrho\bar{\mu}M_c^2 - \bar{\mu}D_c - \bar{\zeta}M_cD_c &= 0. \end{aligned}$$

We wish for D_c to be as close to $D_c^* = 50$ nM. We choose the scale

$$\bar{\mu} = \arg \min_{\mu} |D_c(\mu) - D_c^*|,$$

which is 20.2 s^{-1} . At this optimal μ , the monomer concentration would be $M_c = 71.8 \text{ } \mu\text{M}$ were the clearance to be inhibited. We remark that given the previously established model values and constraints, we were unable to match larger value of D_c , hence the choice of 50 nM instead of 500 nM.

Monomer-Monomer Combination Rate ν : From the two preceding results, we find $\bar{\nu} = 391. \text{ M}^{-1} \text{ s}^{-1}$.

Cross-Referencing the Rate Constants: Experiments measuring $\bar{\mu}$ (60) have found $\bar{\mu} = 12700 \text{ s}^{-1}$. But from experiments observing the conversion of oligomers to monomers, the time scale is on the order of days (so $\bar{\mu} \approx 10^{-5} \text{ s}^{-1}$) (61). The value of $\bar{\mu}$ we find is within the very wide range of estimated values. The value for $\bar{\zeta}$ that we obtain is at least somewhat consistent with $38 \text{ M}^{-1} \text{ s}^{-1}$ (60) only out by a factor of 23. Our estimate for $\bar{\nu}$ is quite different from some estimated values, however. Indeed, it has been estimated as $0.099 \text{ M}^{-1} \text{ s}^{-1}$ (60). However, other combination processes that could be expected to be similar to monomer-monomer interactions have been estimated to have drastically larger rates: monomers are added to fibrils at an estimated rate of $90 \text{ M}^{-1} \text{ s}^{-1}$ (62).

Diffusion Coefficients. Estimates for diffusivities of monomers and dimers are $1.4 \times 10^{-6} \text{ cm}^2/\text{s}$ and $1.1 \times 10^{-6} \text{ cm}^2/\text{s}$, respectively (63). The tortuosity of brain tissue is around 1.6 (64). And the observed diffusivity of a chemical species \mathcal{D}^* is related to its unimpeded diffusivity \mathcal{D} and the tortuosity of its environment ι by

$$\mathcal{D}^* = \mathcal{D}/\iota^2.$$

This results in the diffusivities used in our study.

Supporting Information: Mathematical Details

Here we provide some of the mathematical steps done to arrive at the results presented in the main body of the paper.

Scalings. It is mathematically convenient to work in a dimensionless framework to have better scaled variables and fewer parameters. A dimensionless framework also allows “small” terms to be identified which are used in formal asymptotics to furnish highly accurate but approximate solutions. The equations presented in the main body of the paper have been converted back to dimensional form.

We denote x for spatial position. Within equations Eq. (1), Eq. (2), Eq. (3), and Eq. (8), we perform a change of variables according to

$$\begin{aligned} t &= \bar{t}\tau, x = \bar{x}z \\ M(t) &= \bar{M}m(\tau), D(t) = \bar{D}d(\tau), L(t) = \bar{L}\ell(\tau), V(t) = v(\tau) \\ S &= \bar{S}\bar{s}, \kappa = \bar{\kappa}\bar{\kappa}(\tau), \nu = \bar{\nu}\bar{\nu}(\tau), \mu = \bar{\mu}\bar{\mu}(\tau), \zeta = \bar{\zeta}\bar{\zeta}(\tau), \\ \sigma &= \bar{\sigma}\bar{\sigma}(\tau), \end{aligned}$$

where all overlined values represent dimensional scales, and τ, m, d, v, z , along with all tilde-variables are dimensionless. We remark the rate constants are *allowed to be time-dependent*. We choose the scales $\bar{t} = \bar{\kappa}^{-1}$, $\bar{M} = \bar{S}\bar{t}$, $\bar{D} = \frac{1}{2}\bar{\nu}\bar{t}\bar{M}^2$, and $\bar{x} = \sqrt{\mathcal{D}_M\bar{t}}$. This yields the dimensionless system of equations

$$\frac{\partial m}{\partial \tau} = \Delta_z m + \bar{s} - \bar{\kappa}m - \nu_0(\bar{\nu}m^2 - \bar{\mu}d) - \epsilon\zeta_0 m \bar{\zeta} m d \quad [30]$$

$$\frac{\partial d}{\partial \tau} = \xi^2 \Delta_z d + \epsilon^{-1}(\bar{\nu}m^2 - \bar{\mu}d) - \zeta_0 d \bar{\zeta} m d \quad [31]$$

$$\frac{d\ell}{d\tau} = \epsilon\zeta_0 \bar{\zeta} m d \quad [32]$$

$$\frac{dv}{d\tau} = -\epsilon\sigma_0 \bar{\sigma} v \quad [33]$$

Parameter	Definition	Value
ϵ	$\frac{\bar{\kappa}}{\bar{\mu}}$	7.85×10^{-7}
ν_0	$\frac{\bar{\nu}\bar{S}}{\bar{\kappa}^2}$	9.65
$\zeta_0 m$	$\frac{\bar{\zeta}\bar{\nu}\bar{S}^2}{2\bar{\kappa}^4}$	20.9
$\zeta_0 d$	$\frac{\bar{\zeta}\bar{S}}{\bar{\kappa}^2}$	4.33
$\zeta_0 \ell$	$\frac{\bar{\zeta}\bar{\nu}u\bar{S}^3}{2\bar{\kappa}^5 L}$	8.19
σ_0	$\frac{\bar{\sigma}\bar{\nu}\bar{S}^2}{2\bar{\kappa}^4}$	0.102
ξ	$\sqrt{\frac{\mathcal{D}_D}{\mathcal{D}_M}}$	0.887

Table 3. Dimensionless parameters. With $\epsilon \ll 1$ chosen these serve as constants for the asymptotic calculations.

with values appearing in Table 3. The use of $0 < \epsilon \ll 1$ is suggestive of formal asymptotics.

ODEs. We first consider equations Eq. (30)-Eq. (32) in the absence of diffusion so that the equations are ordinary differential equations and we solve them subject to $m(\tau = 0) = d(\tau = 0) = \ell(\tau = 0) = 0$, with an initial concentration of monomers and dimers of zero, and with $v(\tau = 0) = 1$, i.e., the cell viability is initially at its maximum. The method of dominant balance inspires the ansatz

$$m \sim m_0 + o(1), \quad d \sim d_0 + o(1), \quad \ell \sim \ell_1 + o(\epsilon).$$

We deal with v later.

Since the monomer clearance rate and activity of the β -secretase varies over decades (where $\tau = O(1/\epsilon)$), assume a similar behaviour in other rate constants and model this by

$$\begin{aligned} \bar{s}(\tau) &= \bar{s}_s(\epsilon\tau) \\ \bar{\kappa}(\tau) &= \bar{\kappa}_s(\epsilon\tau) \\ \bar{\nu}(\tau) &= \bar{\nu}_s(\epsilon\tau) \\ \bar{\mu}(\tau) &= \bar{\mu}_s(\epsilon\tau) \\ \bar{\zeta}(\tau) &= \bar{\zeta}_s(\epsilon\tau) \\ \bar{\sigma}(\tau) &= \bar{\sigma}_s(\epsilon\tau) \end{aligned}$$

for $O(1)$ functions with $O(1)$ rates of change $\bar{s}_s, \bar{\kappa}_s, \bar{\nu}_s, \bar{\mu}_s$, and $\bar{\sigma}_s$, i.e., we assume all the rates change over a slow, $O(1/\epsilon)$ timescale.

The system admits multiple time scales but our approach is to treat the system as a set of inner-outer matching problems. Over a very fast time scale, $\tau_f = \tau/\epsilon$, the ODEs are

$$\begin{aligned} m_{0,\tau_f} &= 0 \\ d_{0,\tau_f} &= \bar{\nu}m_0^2 - \bar{\mu}d_0 \\ \ell_{1,\tau_f} &= 0 \end{aligned}$$

so that from our initial conditions, $m_0(\tau_f) = d_0(\tau_f) = \ell_0(\tau_f) = 0$ and nothing eventful happens (to see finer grained behaviour, we could have chosen $m = O(\epsilon)$, etc., but this understanding is not relevant). Over the “normal” timescale we have

$$\begin{aligned} m_{0,\tau} &= \bar{s}_s(0) - \bar{\kappa}_s(0)m_0 - \mu_0(\bar{\nu}_s(0)m_0^2 - \bar{\mu}_s(0)d_0) \\ 0 &= \bar{\nu}_s(0)m_0^2 - \bar{\mu}_s(0)d_0 \\ \ell_{1,\tau} &= \zeta_0, \ell \bar{\zeta}_s(0)m_0 d_0 \end{aligned}$$

which can be trivially matched to the innermost τ_f -region with

$$m_0 = \frac{\bar{s}_s(0)}{\bar{\kappa}_s(0)}(1 - e^{-\bar{\kappa}_s(0)\tau}) \quad [34]$$

$$d_0 = \frac{\bar{\nu}_s(0)}{\bar{\mu}_s(0)}m_0^2 \quad [35]$$

$$\begin{aligned} \ell_1 &= \zeta_0, \ell \frac{\bar{\zeta}_s(0)\bar{\nu}_s(0)\bar{s}_s^3(0)}{\bar{\mu}_s(0)\bar{\kappa}_s^3(0)} \left(\tau + \frac{3}{\bar{\kappa}_s(0)}(e^{-\bar{\kappa}_s(0)\tau} - 1) \right. \\ &\quad \left. - \frac{3}{2\bar{\kappa}_s(0)}(e^{-2\bar{\kappa}_s(0)\tau} - 1) + \frac{1}{3\bar{\kappa}_s(0)}(e^{-3\bar{\kappa}_s(0)\tau} - 1) \right) \quad [36] \end{aligned}$$

In order to observe the system response to changing rate constants, we consider a slow timescale $\tau_s = \epsilon\tau$, now with $\ell \sim \ell_0$. On this timescale we obtain

$$\begin{aligned} 0 &= \tilde{s}_s(\tau_s) - \tilde{\kappa}_s(\tau_s)m_0 - \mu_0(\tilde{\nu}(\tau_s)m_0^2 - \tilde{\mu}(\tau_s)d_0) \\ 0 &= \tilde{\nu}(\tau_s)m_0^2 - \tilde{\mu}(\tau_s)d_0 \\ \ell_{0,\tau_s} &= \zeta_{0,\ell}\tilde{\zeta}(\tau_s)m_0(\tau_s)d_0(\tau_s). \end{aligned}$$

The first two equations do not have explicit τ_s -derivatives: they are a system of algebraic equations that come about through the long-time evolution of Eq. (34)-Eq. (35). The other can be solved trivially by integration to give

$$m_0 = \frac{\tilde{s}_s(\tau_s)}{\tilde{\kappa}_s(\tau_s)} \quad [37]$$

$$d_0 = \frac{\tilde{\nu}_s(\tau_s)\tilde{s}_s^2(\tau_s)}{\tilde{\mu}_s(\tau_s)\tilde{\kappa}_s^2(\tau_s)} \quad [38]$$

$$\ell_0 = \zeta_{0,\ell} \int_0^{\tau_s} \frac{\tilde{\zeta}_s(u)\tilde{\nu}_s(u)\tilde{s}_s^3(u)}{\tilde{\mu}_s(u)\tilde{\kappa}_s^3(u)} du. \quad [39]$$

A composite solution on $t \lesssim 1/\epsilon$ can be obtained as

$$m \sim \frac{\tilde{s}(\tau)}{\tilde{\kappa}(\tau)} - \frac{\tilde{s}(0)}{\tilde{\kappa}(0)} e^{-\tilde{\kappa}(0)\tau} \quad [40]$$

$$d \sim \frac{\tilde{\nu}(\tau)}{\tilde{\mu}(\tau)} \left(\frac{\tilde{s}(\tau)}{\tilde{\kappa}(\tau)} - \frac{\tilde{s}(0)}{\tilde{\kappa}(0)} e^{-\tilde{\kappa}(0)\tau} \right)^2 \quad [41]$$

$$\begin{aligned} \ell &\sim \epsilon\zeta_{0,\ell} \int_0^{\tau} \frac{\tilde{\nu}(u)\tilde{s}^3(u)}{\tilde{\mu}(u)\tilde{\kappa}^3(u)} du \\ &+ \epsilon\zeta_{0,\ell} \frac{\tilde{\zeta}(0)\tilde{\nu}(0)\tilde{s}^3(0)}{\tilde{\mu}(0)\tilde{\kappa}^3(0)} \left(\frac{3}{\tilde{\kappa}(0)} (e^{-\tilde{\kappa}(0)\tau} - 1) \right. \\ &\left. - \frac{3}{2\tilde{\kappa}(0)} (e^{-2\tilde{\kappa}(0)\tau} - 1) + \frac{1}{3\tilde{\kappa}(0)} (e^{-3\tilde{\kappa}(0)\tau} - 1) \right). \end{aligned} \quad [42]$$

From Eq. (33), we have that

$$v(\tau) = \exp\left(-\epsilon\sigma_0 \int_0^{\tau} \tilde{\sigma}(u)(d_0(u) + o(1))du\right)$$

This can be evaluated to

$$v(\tau) = \begin{cases} 1 - \epsilon\sigma_0 \frac{\tilde{\sigma}(0)\tilde{\nu}(0)}{\tilde{\mu}(0)} \left(\frac{\tilde{s}(0)^2}{\tilde{\kappa}(0)^2} \tau + \frac{2\tilde{s}(0)}{\tilde{\kappa}(0)^2} (e^{-\tilde{\kappa}(0)\tau} - 1) \right. \\ \left. + \frac{1}{2\tilde{\kappa}(0)} (e^{-2\tilde{\kappa}(0)\tau} - 1) \right) + o(\epsilon), & \tau = O(1) \\ \exp\left(-\sigma_0 \int_0^{\epsilon\tau} \frac{\tilde{\sigma}_s(u)\tilde{\nu}_s(u)\tilde{s}_s^2(u)}{\tilde{\mu}_s(u)\tilde{\kappa}_s^2(u)} du\right) + o(1), & \tau = O(1/\epsilon). \end{cases} \quad [43]$$

We focus on an $O(1)$ description of v so that a uniformly valid approximation for $\tau \lesssim 1/\epsilon$ is

$$v \sim \exp\left(-\epsilon\sigma_0 \int_0^{\tau} \frac{\tilde{\sigma}(u)\tilde{\nu}(u)\tilde{s}^2(u)}{\tilde{\mu}(u)\tilde{\kappa}^2(u)} du\right). \quad [44]$$

The solutions presented in the main body of the paper are for the biologically relevant timescale of decades, i.e., $\tau = O(1/\epsilon)$.

PDEs. In analyzing the PDE models, there are a number of asymptotic balances that are possible, i.e., depending on the spatial, temporal, or concentration scales that we look at, different terms in the equations dominate the system behaviour. We study one of the most biologically relevant balances.

Throughout this analysis, we will focus upon the local effects of a perturbation in the monomer production. We consider a radially symmetric perturbation so that spherical symmetry and various simplifications can be applied. The solutions presented are obtained from the Green's functions provided later.

Spatial Model Results. We posit $z, \tau = O(1)$, $m \sim m_0 = O(1)$, $d \sim d_0 = O(1)$, and $\tilde{s} = O(1)$. Biologically this describes the system on a length-scale of \bar{X} and a timescale of \bar{T} , with the monomers and dimers being on their characteristic scales \bar{M} and \bar{D} . Denoting $r = |z|$ with the centre of the disturbance at $r = 0$, we have

$$\begin{aligned} m_{0,\tau} &= m_{0,rr} + \frac{2}{r}m_{0,r} + \tilde{s} - \tilde{\kappa}m_0 \\ 0 &= \tilde{\nu}m_0^2 - \tilde{\mu}d_0. \end{aligned}$$

$$\text{If } \tilde{s} = \tilde{s}_0 + \rho \begin{cases} 1, & r < R \\ 0, & r \geq R \end{cases} \text{ then using Eq. (54) and Eq. (53)}$$

with $\alpha = 1$, $\beta = \tilde{\kappa}$, $\phi = \tilde{s}$, we can explicitly solve for m_0 at steady state giving

$$m_0(r) = \frac{\tilde{s}_0}{\tilde{\kappa}} + \rho \begin{cases} \begin{aligned} &\frac{e^{-\sqrt{\tilde{\kappa}}r}}{\sqrt{\tilde{\kappa}}} \left[\frac{r}{\sqrt{\tilde{\kappa}}} \cosh(\sqrt{\tilde{\kappa}}r) - \frac{1}{\tilde{\kappa}} \sinh(\sqrt{\tilde{\kappa}}r) \right] \\ &+ \frac{\sinh(\sqrt{\tilde{\kappa}}r)}{\sqrt{\tilde{\kappa}}} \left[\frac{re^{-\sqrt{\tilde{\kappa}}r}}{\sqrt{\tilde{\kappa}}} - \frac{Re^{-\sqrt{\tilde{\kappa}}R}}{\sqrt{\tilde{\kappa}}} \right] \end{aligned} \\ -\frac{1}{\tilde{\kappa}}e^{-\sqrt{\tilde{\kappa}}R} + \frac{1}{\tilde{\kappa}}e^{-\sqrt{\tilde{\kappa}}r}, & r < R \\ \begin{aligned} &\frac{e^{-\sqrt{\tilde{\kappa}}r}}{\sqrt{\tilde{\kappa}}} \left[\frac{R}{\sqrt{\tilde{\kappa}}} \cosh(\sqrt{\tilde{\kappa}}R) - \frac{1}{\tilde{\kappa}} \sinh(\sqrt{\tilde{\kappa}}R) \right], \\ &r \geq R, \end{aligned} \end{cases} \quad [45]$$

and

$$d_0 = \frac{\tilde{\nu}}{\tilde{\mu}} m_0^2. \quad [46]$$

The fact that we only consider the steady-state here is motivated by our observation in the ODE model that over an $O(1)$ time in τ , the viability loss is $O(\epsilon)$, which is negligible. The most important dynamics occur over the τ_s timescale whereby m_0 and d_0 can be taken as steady-state values.

Solutions via Green's Functions. The preceding solutions were obtained using Green's functions. In general to solve the spherically symmetric problem

$$h_t = \alpha(h_{rr} + \frac{2}{r}h_r) - \beta h + \phi(r, t) \quad [47]$$

$$h(r, 0) = h_0(r) \quad [48]$$

$$h(\infty, t) \text{ is bounded, } h_r(0, t) = 0 \quad [49]$$

we find that

$$h(r, t) = \int_0^\infty \int_0^\infty r^{*2} \phi(r^*, t^*) G(r^*, t^*; r, t) dr^* dt^* \quad [50]$$

$$+ \int_0^\infty r^{*2} h_0(r^*) G(r^*, 0; r, t) dr^* \quad [51]$$

where

$$\begin{aligned} G(r^*, t^*; r, t) &= \frac{\Theta(t-t^*)}{2\sqrt{\pi\alpha(t-t^*)rr^*}} \\ &\times \left(e^{-\frac{(r-r^*)^2}{4\alpha(t-t^*)}} - e^{-\frac{(r+r^*)^2}{4\alpha(t-t^*)}} \right) e^{-\beta(t-t^*)}. \end{aligned} \quad [52]$$

The function Θ denotes the Heaviside step function,

$$\Theta(x) = \begin{cases} 1, & x \geq 0 \\ 1/2, & x = 0 \\ 0, & x < 0. \end{cases}$$

Also, if ϕ does not depend on time, the steady-state solution can be found from

$$h(r) = \int_0^\infty r^{*2} G(r^*; r) \phi(r^*) dr^* \quad [53]$$

with G now given by

$$G(r^*; r) = \begin{cases} \frac{1}{2\sqrt{\alpha\beta rr^*}} (e^{-\sqrt{\beta/\alpha}(r-r^*)} - e^{-\sqrt{\beta/\alpha}(r+r^*)}), & r^* < r \\ \frac{1}{2\sqrt{\alpha\beta rr^*}} (e^{-\sqrt{\beta/\alpha}(r^*-r)} - e^{-\sqrt{\beta/\alpha}(r+r^*)}), & r^* > r. \end{cases} \quad [54]$$

Supporting Information: Average \bar{U} within AD Patients

We consider the possibility that even within the static model, \bar{U} has a distribution of values within the population. We suppose that $\bar{U} \sim g(u)$ with g being the probability density function (pdf) for U and with $\mathbb{E}(\bar{U}) = U^*$ as the mean value and $\text{Var}(\bar{U}) = \Sigma^{*2}$ as the variance. To exploit various asymptotic approximations, we operate under the assumptions:

- $U^* \sim \Sigma^*$ in the sense they are in the same ballpark of values,
- $\gamma T_D U^*, \gamma T_D \Sigma^* \ll 1$, and
- $g(u)$ is exponentially small when $\gamma T_D u \geq O(1)$.

In practice many distributions fit this requirement. For example, g could be a truncated (to disallow negative values) Gaussian distribution with mean U^* and variance U^{*2} , where $\gamma U^* T_D \ll 1$.

We wish to understand if the average value of \bar{U} among those with AD is higher than U^* , i.e., *if those with AD may have a larger rate of neuronal loss, on average*. To this end, we seek the density

$$g_{AD^+}(u) = \frac{\Pr(\text{AD at age } t | \bar{U} = u)g(u)}{\int_0^\infty g(u) \Pr(\text{AD at age } t | \bar{U} = u)du}.$$

Colloquially, it is the pdf for \bar{U} given that someone has AD. We wish to understand if

$$\langle \bar{U} \rangle_{AD^+} = \int_0^\infty u g_{AD^+}(u) du$$

is larger than U^* , the mean value of \bar{U} .

Under a static model, $\Pr(\text{AD at age } t | \bar{U} = u) = 1 - \exp(-\gamma T_D u)$ is the prevalence of AD with $\bar{U} = u$, which, by Taylor series, is approximately $\gamma T_D u$, for small enough $\gamma T_D u$. Thus, with formal asymptotics,

$$\begin{aligned} \langle \bar{U} \rangle_{AD^+} &\sim \int_0^\infty \frac{\gamma T_D u^2 g(u)}{\int_0^\infty \gamma T_D w g(w) dw} du = \frac{1}{\mathbb{E}(\bar{U})} \int_0^\infty u^2 g(u) du \\ &= \frac{\mathbb{E}(\bar{U}^2)}{\mathbb{E}(\bar{U})} = U^* + \frac{\Sigma^{*2}}{U^*} > U^*. \end{aligned}$$

We have used $\text{Var}(\bar{U}) = \mathbb{E}(\bar{U}^2) - \mathbb{E}(\bar{U})^2$.

We can also compute the expected value of \bar{U} given someone does not have AD. We denote AD^- to be the case AD is absent. Using similar notation and approximations, we have

$$g_{AD^-}(u) = \frac{\Pr(\text{no AD at age } t | \bar{U} = u)g(u)}{\int_0^\infty g(u) \Pr(\text{no AD at age } t | \bar{U} = u)du}$$

with

$$\begin{aligned} \langle \bar{U} \rangle_{AD^-} &\sim \int_0^\infty \frac{(u - \gamma T_D u^2)g(u)}{\int_0^\infty (1 - \gamma T_D w)g(w)dw} du \\ &= \frac{\mathbb{E}(\bar{U}) - \gamma T_D \mathbb{E}(\bar{U}^2)}{1 - \gamma T_D \mathbb{E}(\bar{U})} \\ &\sim U^* - \gamma T_D \Sigma^{*2} + O(\gamma^2 T_D^2 \bar{U}^2). \end{aligned}$$

To leading order, this is U^* .

As a check, we have that

$$\begin{aligned} \mathbb{E}(\bar{U}) &= \mathbb{E}(\bar{U} | AD^+) \Pr(AD^+) + \mathbb{E}(\bar{U} | AD^-) \Pr(AD^-) \\ &\sim (U^* + \frac{\Sigma^{*2}}{U^*}) \int_0^\infty g(u) \gamma u T_D \\ &\quad + (U^* - \gamma T_D \Sigma^{*2}) \int_0^\infty g(u) (1 - \gamma u T_D) du \\ &= (U^* + \frac{\Sigma^{*2}}{U^*}) \gamma U^* T_D + (U^* - \gamma T_D \Sigma^{*2}) (1 - \gamma \bar{U} T_D) \\ &= U^* (1 + O(\gamma^2 \Sigma^{*2} T_D^2)) \end{aligned}$$

1. Kochanek KD, Murphy SL, Xu J, Tejada-Vera B (2019) Deaths: Final data for 2014. *National Vital Statistics Reports* 65(4):1–121.
2. Cummings J, Lee G, Ritter A, Sabbagh M, Zhong K (2019) Alzheimer's disease drug development pipeline: 2019. *Alzheimer's & Dementia: Translational Research & Clinical Interventions* 5:272–293.

3. Hardy JA, Higgins GA (1992) Alzheimer's disease: the amyloid cascade hypothesis. *Science* 256:184–185.
4. Ono K, Condron MM, Teplow DB (2009) Structure-neurotoxicity relationships of amyloid β -protein oligomers. *Proceedings of the National Academy of Sciences USA* 106(35):14745–14750.
5. Roychaudhuri R, Yang M, Hoshi MM, Teplow DB (2009) Amyloid β -Protein Assembly and Alzheimer Disease. *Journal of Biological Chemistry* 284(8):4749–4753.
6. Shankar GM, et al. (2008) Amyloid-beta protein dimers isolated directly from Alzheimer's brains impair synaptic plasticity and memory. *Nature Medicine* 14(8):837–842.
7. Cline EN, Bicca MA, Viola KL, Klein WL (2018) The Amyloid- β Oligomer Hypothesis: Beginning of the Third Decade. *J Alzheimer's Disease* 64(s1):S67–S610.
8. Chen XQ, Mobley WC (2019) Alzheimer Disease Pathogenesis: Insights From Molecular and Cellular Biology Studies of Oligomeric A β and Tau Species. *Frontiers in Neuroscience* 13:659–659.
9. Hayden E, Teplow DB (2013) Amyloid β -protein oligomers and Alzheimer's disease. *Alzheimer's Res Ther* 5(6):60.
10. Greenwald J, Riek R (2010) Biology of amyloid: Structure, function, and regulation. *Structure* 18(10):1244–1260.
11. Xiao Y, et al. (2015) A β (1–42) fibril structure illuminates self-recognition and replication of amyloid in Alzheimer's disease. *Nature Structural & Molecular Biology* 22(6):499–507.
12. Chuang E, Hori AM, Hesketh CD, Shorter J (2018) Amyloid assembly and disassembly. *Journal of Cell Science* 131(8).
13. Cheon MS, Dierssen M, Kim SH, Lubec G (2008) Protein expression of bace1, bace2 and app in down syndrome brains. *Amino Acids* 35(2):339–343.
14. O'Brien RJ, Wong PC (2011) Amyloid precursor protein processing and Alzheimer's disease. *Annual Review of Neuroscience* 34:185–204.
15. (2019) Alzheimer's disease fact sheet.
16. Ferri CP, et al. (2005) Global prevalence of dementia: a delphi consensus study. *The Lancet* 366(9503):2112–2117.
17. Hebert LE, Weuve J, Scherr PA, Evans DA (2013) Alzheimer disease in the United States (2010–2050) estimated using the 2010 census. *Neurology* 80(19):1778–1783.
18. Yamazaki Y, Zhao N, Caulfield TR, Liu CC, Bu G (2019) Apolipoprotein E and Alzheimer disease: pathobiology and targeting strategies. *Nature Reviews Neurology* p. 1.
19. Mendez M (2017) What is the relationship of traumatic brain injury to dementia? *J Alzheimer's Disease* 57:667–681.
20. Turner RC, Lucke-Wold BP, Robson MJ, Lee JM, Bailes JE (2016) Alzheimer's disease and chronic traumatic encephalopathy: Distinct but possibly overlapping disease entities. *Brain Injury* 30(11):1279–1292.
21. Das R, et al. (2011) Modeling effect of a γ -secretase inhibitor on amyloid- β dynamics reveals significant role of an amyloid clearance mechanism. *Bulletin of Mathematical Biology* 73(1):230–247.
22. Luca M, Chavez-Ross A, Edelstein-Keshet L, Mogilner A (2003) Chemotactic signaling, microglia, and Alzheimer's disease senile plaques: Is there a connection? *Bulletin of Mathematical Biology* 65(4):693–730.
23. Puri IK, Li L (2010) Mathematical modeling for the pathogenesis of Alzheimer's disease. *PLoS One* 5(12):e15176.
24. Hao W, Friedman A (2016) Mathematical model on Alzheimer's disease. *BMC Systems Biology* 10(1):108.
25. Winter F, Bludszuweit-Philipp C, Wolkenhauer O (2018) Mathematical analysis of the influence of brain metabolism on the BOLD signal in Alzheimer's disease. *Journal of Cerebral Blood Flow & Metabolism* 38(2):304–316.
26. Schmidt V, et al. (2012) Quantitative modelling of amyloidogenic processing and its influence by SORLA in Alzheimer's disease. *The EMBO journal* 31(1):187–200.
27. Bertsch M, Franchi B, Marcello N, Tesi MC, Tosin A (2016) Alzheimer's disease: a mathematical model for onset and progression. *Mathematical Medicine and Biology: a Journal of the IMA* 34(2):193–214.
28. Lloret-Villas A, et al. (2017) The impact of mathematical modeling in understanding the mechanisms underlying neurodegeneration: evolving dimensions and future directions. *CPT: Pharmacometrics & Systems Pharmacology* 6(2):73–86.
29. Urbanc B, Cruz Cruz L, Teplow D, Stanley H (2007) Computer simulations of Alzheimer's amyloid beta-protein folding and assembly. *Current Alzheimer Research* 3:493–504.
30. Urbanc B, et al. (2004) In silico study of amyloid β -protein folding and oligomerization. *Proceedings of the National Academy of Sciences of the United States of America* 101(50):17345–17350.
31. Bernstein MA, Griffin J (2006) Regional differences in the price-elasticity of demand for energy, (National Renewable Energy Lab.(NREL), Golden, CO (United States)), Technical report.
32. Lambert MP, et al. (1998) Diffusible, nonfibrillar ligands derived from A β 1–42 are potent central nervous system neurotoxins. *Proceedings of the National Academy of Sciences* 95(11):6448–6453.
33. Cizas P, et al. (2010) Size-dependent neurotoxicity of β -amyloid oligomers. *Archives of Biochemistry and Biophysics* 496(2):84–92.
34. Rinne H (2014) *The Hazard rate: Theory and inference (with supplementary MATLAB-Programs)*.
35. Del Ferraro G, et al. (2018) Finding influential nodes for integration in brain networks using optimal percolation theory. *Nature Communications* 9(1):2274.
36. Moghekar A, et al. (2011) Large quantities of A β peptide are constitutively released during amyloid precursor protein metabolism in vivo and in vitro. *Journal of Biological Chemistry* 286(18):15989–15997.
37. Christensen JR, et al. (2007) Neocortical and hippocampal neuron and glial cell numbers in the rhesus monkey. *The Anatomical Record: Advances in Integrative Anatomy and Evolutionary Biology: Advances in Integrative Anatomy and Evolutionary Biology* 290(3):330–340.
38. Fukumoto H, et al. (2004) β -secretase activity increases with aging in human, monkey, and mouse brain. *The American Journal of Pathology* 164(2):719–725.

39. Fukumoto H, Cheung BS, Hyman BT, Irizarry MC (2002) β -Secretase protein and activity are increased in the neocortex in Alzheimer disease. *Archives of Neurology* 59(9):1381–1389.
40. Nistor M, et al. (2007) Alpha- and beta-secretase activity as a function of age and beta-amyloid in down syndrome and normal brain. *Neurobiology of Aging* 28(10):1493–1506.
41. Lue LF, et al. (1999) Soluble amyloid β peptide concentration as a predictor of synaptic change in Alzheimer's disease. *The American Journal of Pathology* 155(3):853–862.
42. Raskatov JA (2019) What is the "relevant" amyloid β 42 concentration? *ChemBioChem*.
43. Fitzpatrick AL, Kuller LH, Lopez OL, Kawas CH, Jagust W (2005) Survival following dementia onset: Alzheimer's disease and vascular dementia. *Journal of the Neurological Sciences* 229:43–49.
44. The World Bank (2019) Life expectancy. data retrieved from The World Bank, https://data.worldbank.org/indicator/SP.DYN.LE00.IN?cid=GPD_10&locations=US.
45. Patterson BW, et al. (2015) Age and amyloid effects on human central nervous system amyloid-beta kinetics. *Annals of Neurology* 78(3):439–453.
46. Desikan RS, et al. (2017) Genetic assessment of age-associated Alzheimer disease risk: Development and validation of a polygenic hazard score. *PLoS medicine* 14(3):e1002258.
47. Wisniewski K, Wisniewski H, Wen G (1985) Occurrence of neuropathological changes and dementia of Alzheimer's disease in Down's syndrome. *Annals of Neurology: Official Journal of the American Neurological Association and the Child Neurology Society* 17(3):278–282.
48. Wiseman FK, et al. (2015) A genetic cause of Alzheimer disease: mechanistic insights from Down syndrome. *Nature Reviews Neuroscience* 16(9):564–574.
49. Doherty BM, et al. (2015) Amyloid burden, cortical thickness, and cognitive function in the Wisconsin Registry for Alzheimer's Prevention. *Alzheimer's & Dementia: Diagnosis, Assessment & Disease Monitoring* 1(2):160–169.
50. Gordon BA, et al. (2016) Longitudinal β -amyloid deposition and hippocampal volume in pre-clinical Alzheimer disease and suspected non-Alzheimer disease pathophysiology. *JAMA Neurology* 73(10):1192–1200.
51. Starkstein SE, Jorge R (2005) Dementia after traumatic brain injury. *International Psychogeriatrics* 17(s1):S93–S107.
52. Fann JR, et al. (2018) Long-term risk of dementia among people with traumatic brain injury in denmark: a population-based observational cohort study. *The Lancet Psychiatry* 5(5):424–431.
53. McKee AC, et al. (2009) Chronic traumatic encephalopathy in athletes: progressive tauopathy after repetitive head injury. *Journal of Neuropathology & Experimental Neurology* 68(7):709–735.
54. Johnson VE, Stewart W, Smith DH (2010) Traumatic brain injury and amyloid- β pathology: a link to Alzheimer's disease? *Nature Reviews Neuroscience* 11(5):361.
55. Akaike H (1974) A new look at the statistical model identification in *Selected Papers of Hirotugu Akaike*. (Springer), pp. 215–222.
56. Pistollato F, et al. (2016) Associations between sleep, cortisol regulation, and diet: possible implications for the risk of Alzheimer disease. *Advances in Nutrition* 7(4):679–689.
57. Smith AJ, Verkman AS (2017) The "glymphatic" mechanism for solute clearance in Alzheimer's disease: game changer or unproven speculation? *The FASEB Journal* 32(2):543–551.
58. Norden R (1972) A survey of maximum likelihood estimation. *International Statistical Review/Revue Internationale de Statistique* pp. 329–354.
59. Jin M, et al. (2011) Soluble amyloid β -protein dimers isolated from Alzheimer cortex directly induce Tau hyperphosphorylation and neuritic degeneration. *Proceedings of the National Academy of Sciences* 108(14):5819–5824.
60. Garai K, Frieden C (2013) Quantitative analysis of the time course of $\alpha\beta$ oligomerization and subsequent growth steps using tetramethylrhodamine-labeled $\alpha\beta$. *Proceedings of the National Academy of Sciences* 110(9):3321–3326.
61. Nag S, et al. (2011) Nature of the amyloid- β monomer and the monomer-oligomer equilibrium. *Journal of Biological Chemistry* 286(16):13827–13833.
62. Lomakin A, Teplow DB, Kirschner DA, Benedek GB (1997) Kinetic theory of fibrillogenesis of amyloid β -protein. *Proceedings of the National Academy of Sciences* 94(15):7942–7947.
63. Murphy RM, Pallitto MM (2000) Probing the kinetics of β -amyloid self-association. *Journal of Structural Biology* 130(2-3):109–122.
64. Mériaux S, Conti A, Larrat B (2018) Assessing diffusion in the extra-cellular space of brain tissue by dynamic mri mapping of contrast agent concentrations. *Frontiers in Physics* 6:38.